Supplementary Information for
A versatile, phase coherent data acquisition system based on software-defined radio for graphene nanomechanics

Ce Zhang,[1,2] YuBin Zhang,[1,2] Chen Yang,[1,2] Heng Lu,[1,2]
FengNan Chen,[1,2] Ying Yan,[1,2] and Joel Moser[1,2,*]

[1]*School of Optoelectronic Science and Engineering & Collaborative Innovation Center of Suzhou Nano Science and Technology, Soochow University, Suzhou 215006, China*

[2]*Key Lab of Advanced Optical Manufacturing Technologies of Jiangsu Province & Key Lab of Modern Optical Technologies of Education Ministry of China, Soochow University, Suzhou 215006, China*

CONTENTS

* j.moser@suda.edu.cn

I. NOTATION

δz_{m}	complex amplitude of flexural vibrations
ϕ_{m}	phase of vibrations with respect to phase of drive
f_{m}	resonant frequency of vibration mode
k_{m}	spring constant of vibration mode
Q_{m}	quality factor of vibration mode
m_{eff}	effective mass of vibration mode
η	nonlinear damping factor of vibration mode
C_{g}	capacitance between resonator and gate
$V_{\mathrm{g}}^{\mathrm{dc}}$	dc voltage applied between resonator and gate
δV_{d}	rms amplitude of coherent ac voltage applied between resonator and gate
P_{d}	drive power applied to source of resonator
δF_{d}	rms amplitude of coherent driving force
f_{d}	frequency of coherent driving force
S	single-sided power spectral density
P	power calculated as S multiplied by bandwidth
$\langle\cdot\rangle_m$	average of m realizations
$\mathbb{V}$	variance
$4S_{uu}$	intensity of voltage noise applied to the source of the resonator
$h(t) \leftrightarrow \hat{H}(f)$	Fourier transform from time to frequency
f	Fourier or spectral frequency
I, Q	in-phase and quadrature components of vibrations
$V_{\mathrm{pd}}(t)$	photodetector output voltage
$\tilde{I}$, $\tilde{Q}$	in-phase and quadrature components of downconverted $V_{\mathrm{pd}}(t)$
κ	spring constant modulation strength
f_{mod}	spring constant modulation frequency
ρ	Fresnel reflection coefficient
d	distance or thickness
λ	wavelength
R	reflectance
A	absorbance

II. ESTIMATING THE THICKNESS OF THE FEW-LAYER GRAPHENE MEMBRANE

We estimate the thickness of the resonator using optical reflectometry. Namely, we measure the reflectance of the system composed of few-layer graphene (FLG) in contact with the substrate of silicon oxide coated silicon (hereafter R_{FLG}) and the reflectance of the substrate without FLG (hereafter R_{bare}). We then calculate R_{FLG} and R_{bare} within a model of normally incident plane waves [1]. We find $R_{\mathrm{FLG}} = |c/a|^2$ and $R_{\mathrm{bare}} = |c'/a'|^2$, with

$$\begin{bmatrix} a \\ c \end{bmatrix} = \frac{1}{1+\rho_1} \begin{bmatrix} 1 & \rho_1 \\ \rho_1 & 1 \end{bmatrix} \begin{bmatrix} e^{\mathrm{j}\frac{2\pi}{\lambda} n_{\mathrm{G}} d_{\mathrm{G}}} & 0 \\ 0 & e^{-\mathrm{j}\frac{2\pi}{\lambda} n_{\mathrm{G}} d_{\mathrm{G}}} \end{bmatrix} \cdot \frac{1}{1+\rho_2} \begin{bmatrix} 1 & \rho_2 \\ \rho_2 & 1 \end{bmatrix} \begin{bmatrix} e^{\mathrm{j}\frac{2\pi}{\lambda} n_{\mathrm{ox}} d_{\mathrm{ox}}} & 0 \\ 0 & e^{-\mathrm{j}\frac{2\pi}{\lambda} n_{\mathrm{ox}} d_{\mathrm{ox}}} \end{bmatrix} \frac{1}{1+\rho_3} \begin{bmatrix} 1 & \rho_3 \\ \rho_3 & 1 \end{bmatrix} \begin{bmatrix} 1 \\ 0 \end{bmatrix} \tag{1}$$

and with

$$\begin{bmatrix} a' \\ c' \end{bmatrix} = \frac{1}{1+\rho_1'} \begin{bmatrix} 1 & \rho_1' \\ \rho_1' & 1 \end{bmatrix} \begin{bmatrix} e^{\mathrm{j}\frac{2\pi}{\lambda} n_{\mathrm{ox}} d_{\mathrm{ox}}} & 0 \\ 0 & e^{-\mathrm{j}\frac{2\pi}{\lambda} n_{\mathrm{ox}} d_{\mathrm{ox}}} \end{bmatrix} \frac{1}{1+\rho_3} \begin{bmatrix} 1 & \rho_3 \\ \rho_3 & 1 \end{bmatrix} \begin{bmatrix} 1 \\ 0 \end{bmatrix}, \tag{2}$$

where

$$\begin{aligned} \rho_1 &= \frac{1-n_{\mathrm{G}}}{1+n_{\mathrm{G}}} \\ \rho_2 &= \frac{n_{\mathrm{G}}-n_{\mathrm{ox}}}{n_{\mathrm{G}}+n_{\mathrm{ox}}} \\ \rho_3 &= \frac{n_{\mathrm{ox}}-n_{\mathrm{Si}}}{n_{\mathrm{ox}}+n_{\mathrm{Si}}} \\ \rho_1' &= \frac{1-n_{\mathrm{ox}}}{1+n_{\mathrm{ox}}}\,. \end{aligned}$$

We use the following refractive indices at $\lambda = 633$ nm:

$$\begin{aligned} n_{\mathrm{G}} &= 2.6 - \mathrm{j}1.3 \text{ (graphene)} \\ n_{\mathrm{G}}' &= 2.86 - \mathrm{j}1.73 \text{ (graphene}'\text{)} \\ n_{\mathrm{ox}} &= 1.476 \text{ (SiO}_2\text{)} \\ n_{\mathrm{Si}} &= 3.882 - \mathrm{j}0.0196\,. \end{aligned}$$

The thickness of SiO_2 is $d_{\mathrm{ox}} = 500$ nm and the thickness of FLG is $d_{\mathrm{G}} = N_{\mathrm{L}} \times 0.34$ nm with N_{L} the number of layers. The refractive index for graphene′ is borrowed from Ref. [2]. The refractive index n_{G} used e.g. in Ref [3] yields an absorbance A for free-standing single layer graphene that is close to $\pi\alpha$, where α is the fine structure constant. Indeed, for a single layer we find

$$A = 1 - |c''/a''|^2 - 1/|a''|^2 \simeq \pi\alpha \simeq 0.022\,, \tag{3}$$

with

$$\begin{bmatrix} a'' \\ c'' \end{bmatrix} = \frac{1}{1+\rho_1}\begin{bmatrix} 1 & \rho_1 \\ \rho_1 & 1 \end{bmatrix}\begin{bmatrix} e^{\mathrm{j}\frac{2\pi}{\lambda}n_{\mathrm{G}}d_{\mathrm{G}}} & 0 \\ 0 & e^{-\mathrm{j}\frac{2\pi}{\lambda}n_{\mathrm{G}}d_{\mathrm{G}}} \end{bmatrix}\frac{1}{1-\rho_1}\begin{bmatrix} 1 & -\rho_1 \\ -\rho_1 & 1 \end{bmatrix}\begin{bmatrix} 1 \\ 0 \end{bmatrix}. \tag{4}$$

Figure S1 shows the ratio of calculated R_{FLG} to calculated R_{bare} as a function of the number of graphene layers in the resonator. Both n_{G} and n'_{G} are used. The horizontal dashed line represents the measured ratio. Within our model, we estimate that the resonator is composed of 3 to 4 graphene layers.

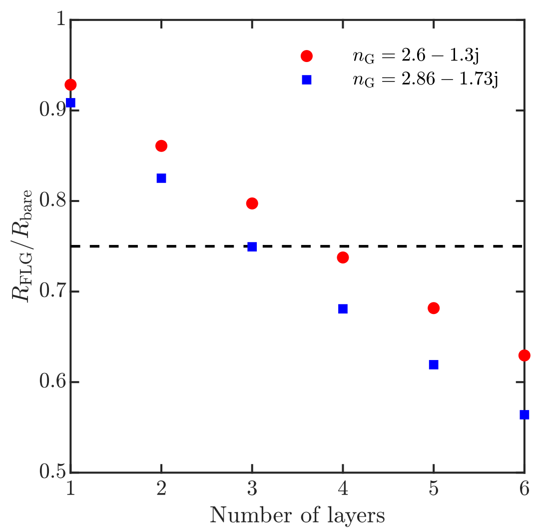

FIG. S1. Estimating the thickness of the resonator. Dots: calculated ratio of R_{FLG} (FLG on SiO_2 on Si) to R_{bare} (SiO_2 on Si) at $\lambda = 633$ nm as a function of the number of layers in FLG. Horizontal dashed line shows the measured ratio.

III. DETAILED MEASUREMENT CIRCUITS

The schematics below show the details of the circuits used for cross-power measurements of driven vibrations (Fig. S2), vibration ringdown (Fig. S3) and measurements of phase modulation induced by strain modulation (Fig. S4).

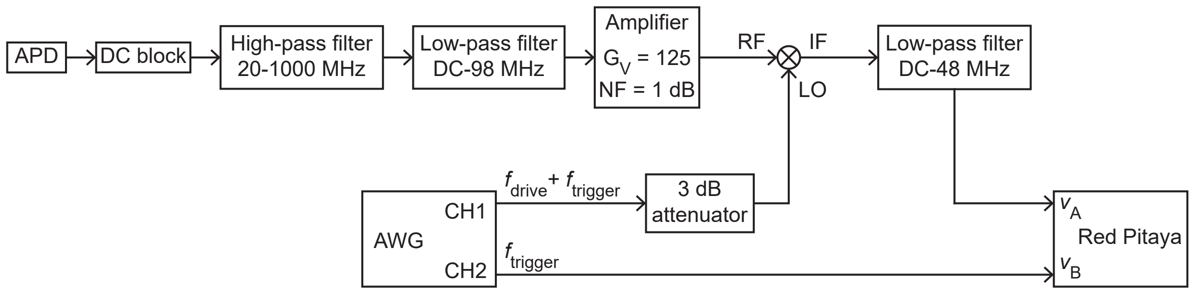

FIG. S2. Cross-power measurement of driven vibrations.

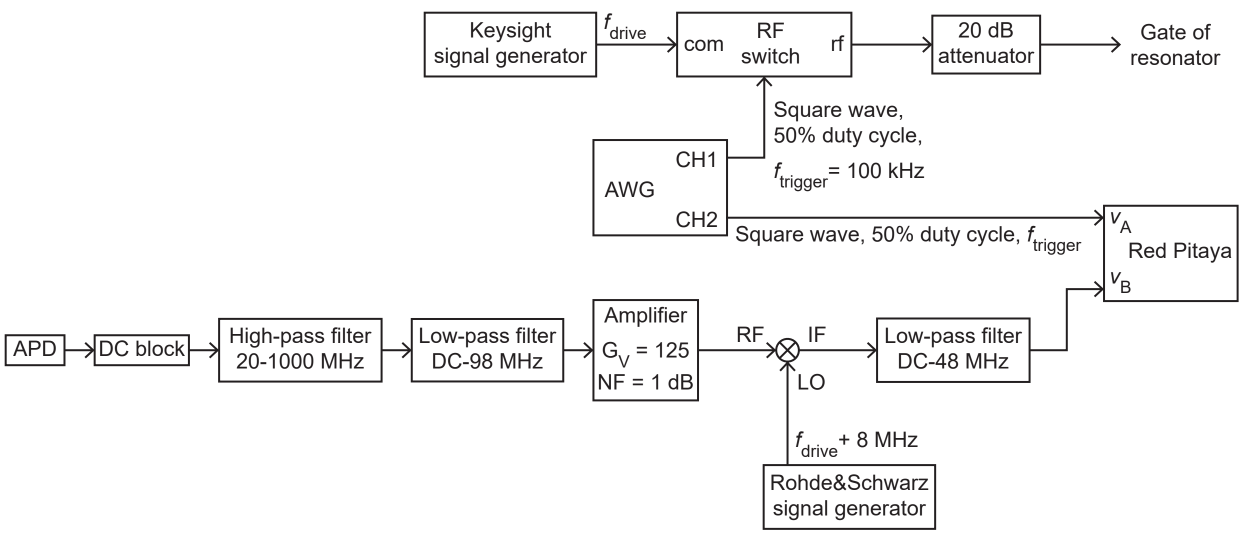

FIG. S3. Ringdown.

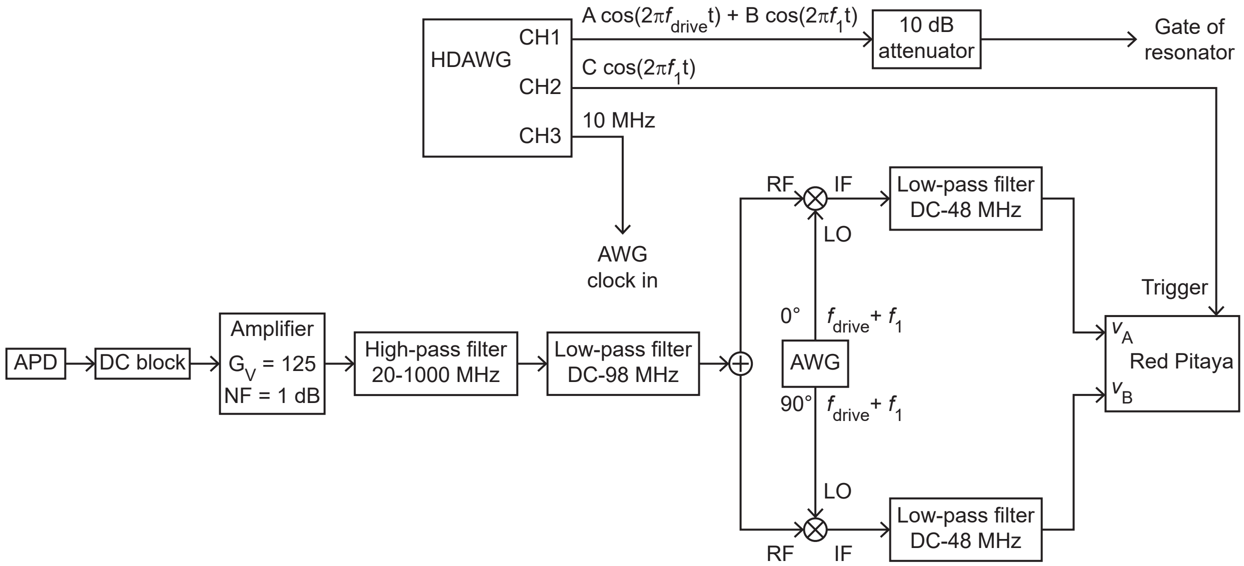

FIG. S4. Phase modulation.

IV. POWER SPECTRA OF DISPLACEMENT FLUCTUATIONS INDUCED BY A FORCE NOISE

Figure S5 shows the averaged single-sided cross-power spectral density of voltage fluctuations measured at nodes v_1 and v_2 (see Fig. 1a in the main text). This averaged spectral density is labeled as $|\langle S_{v_2 v_1}\rangle_m|$ in the main text. It results from the average of $m = 10^5$ cross-power spectral density spectra computed from 10^5 v_1 and v_2 time traces. The intensity of voltage noise $4S_{uu}$ applied to the source of the resonator increases from (a) through (k) (see captions for details). Red traces are fits to Lorentzian lineshapes. Figure S5(l), bottom right panel, shows the full width at half maximum Δf extracted from the Lorentzian fits as a function of S_{uu}. The black trace is a fit of these data to a nonlinear damping model. It is obtained by numerically solving the following equation of motion:

$$\delta\ddot{z}_{\mathrm{m}} + \left[\frac{\omega_{\mathrm{m}}}{Q_{\mathrm{m}}} + \frac{\eta}{m_{\mathrm{eff}}}\delta z_{\mathrm{m}}^2(t)\right]\delta\dot{z}_{\mathrm{m}} + \omega_{\mathrm{m}}^2\delta z_{\mathrm{m}}(t) = \frac{\delta F(t)}{m_{\mathrm{eff}}}\,, \tag{5}$$

with $\delta z_{\mathrm{m}}(t)$ the fluctuating displacement, $\omega_{\mathrm{m}} = 2\pi f_{\mathrm{m}}$ the angular resonant frequency, Q_{m} the quality factor, η the nonlinear damping coefficient, and m_{eff} the effective mass of the mode. $\delta F(t)$ is a fluctuating force that is delta-correlated and whose single-sided power spectral density reads $S_{FF} = 4S_{uu}(C'_{\mathrm{g}}V_{\mathrm{g}}^{\mathrm{dc}})^2$, with $C'_{\mathrm{g}} \simeq 8\times10^{-10}$ F/m the gradient of gate capacitance simulated with COMSOL using the geometry of the device and $V_{\mathrm{g}}^{\mathrm{dc}} = -15$ V the dc voltage between the gate and the resonator. The factor of 4 accounts for the full reflection of radio frequency waves at the resonator due to impedance mismatch. We find that the model reproduces $\Delta f(S_{uu})$ well using $Q_\mathrm{m} = 160$ and $\eta = 0.9 \times 10^{13}$ kg m^{-2} s^{-1}. Please note that, in Fig. S5, S_{uu} is the calibrated power spectral density of voltage fluctuations measured across the 50 Ohm input impedance of a spectrum analyzer.

Figure S6 displays a simulation of Brownian motion based on the geometrical parameters

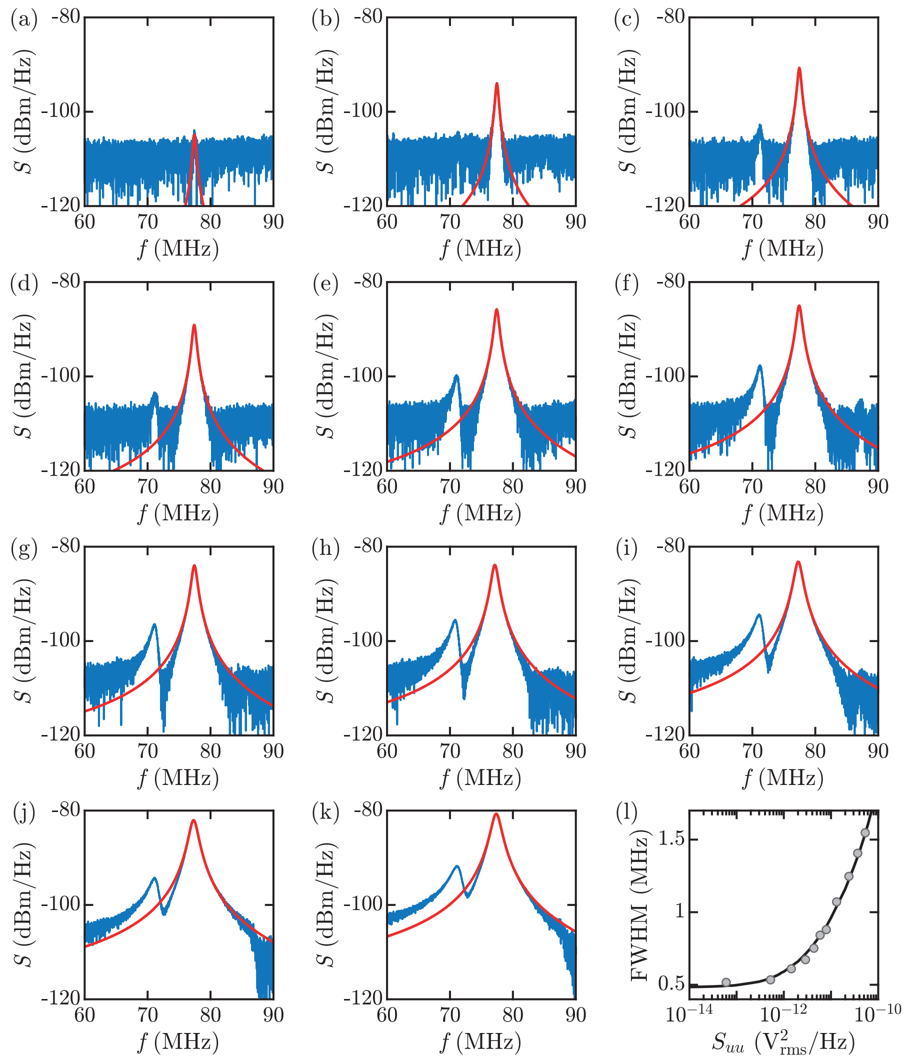

FIG. S5. Averaged single-sided cross-power spectral density of voltage fluctuations $|\langle S_{v_2v_1}\rangle_m|$ with $m = 10^5$. (a)-(k): $S_{uu} \simeq 6\times10^{-14}$ $\mathrm{V^2_{rms}}$/Hz (a); $S_{uu} \simeq 5.2\times10^{-13}$ $\mathrm{V^2_{rms}}$/Hz (b); $S_{uu} \simeq 1.4\times10^{-12}$ $\mathrm{V^2_{rms}}$/Hz (c); $S_{uu} \simeq 2.9\times10^{-12}$ $\mathrm{V^2_{rms}}$/Hz (d); $S_{uu} \simeq 4.3\times10^{-12}$ $\mathrm{V^2_{rms}}$/Hz (e); $S_{uu} \simeq 5.9\times10^{-12}$ $\mathrm{V^2_{rms}}$/Hz (f); $S_{uu} \simeq 7.9\times10^{-12}$ $\mathrm{V^2_{rms}}$/Hz (g); $S_{uu} \simeq 1.3\times10^{-11}$ $\mathrm{V^2_{rms}}$/Hz (h); $S_{uu} \simeq 2.4\times10^{-11}$ $\mathrm{V^2_{rms}}$/Hz (i); $S_{uu} \simeq 3.7\times10^{-11}$ $\mathrm{V^2_{rms}}$/Hz (j); $S_{uu} \simeq 5.3\times10^{-11}$ $\mathrm{V^2_{rms}}$/Hz (k). (l) Measured $\Delta f(S_{uu})$ (dots), and fit based on eq. (5).

of the resonator in the main text. $\langle S_{v_1v_1}\rangle_m$ (light blue) and $|\langle S_{v_2v_1}\rangle_m|$ (dark blue) are shown as a function of Fourier frequency. From a to f, m ranges from 1 to 10^5. The power spectral density of voltage fluctuations is $S_{uu} = -115$ dBm/Hz $= 1.58 \times 10^{-13}$ $\mathrm{V^2_{rms}}$/Hz. The simulation is based on the formalism developed in Ref. [4]. We find that it reproduces the measured spectrum well.

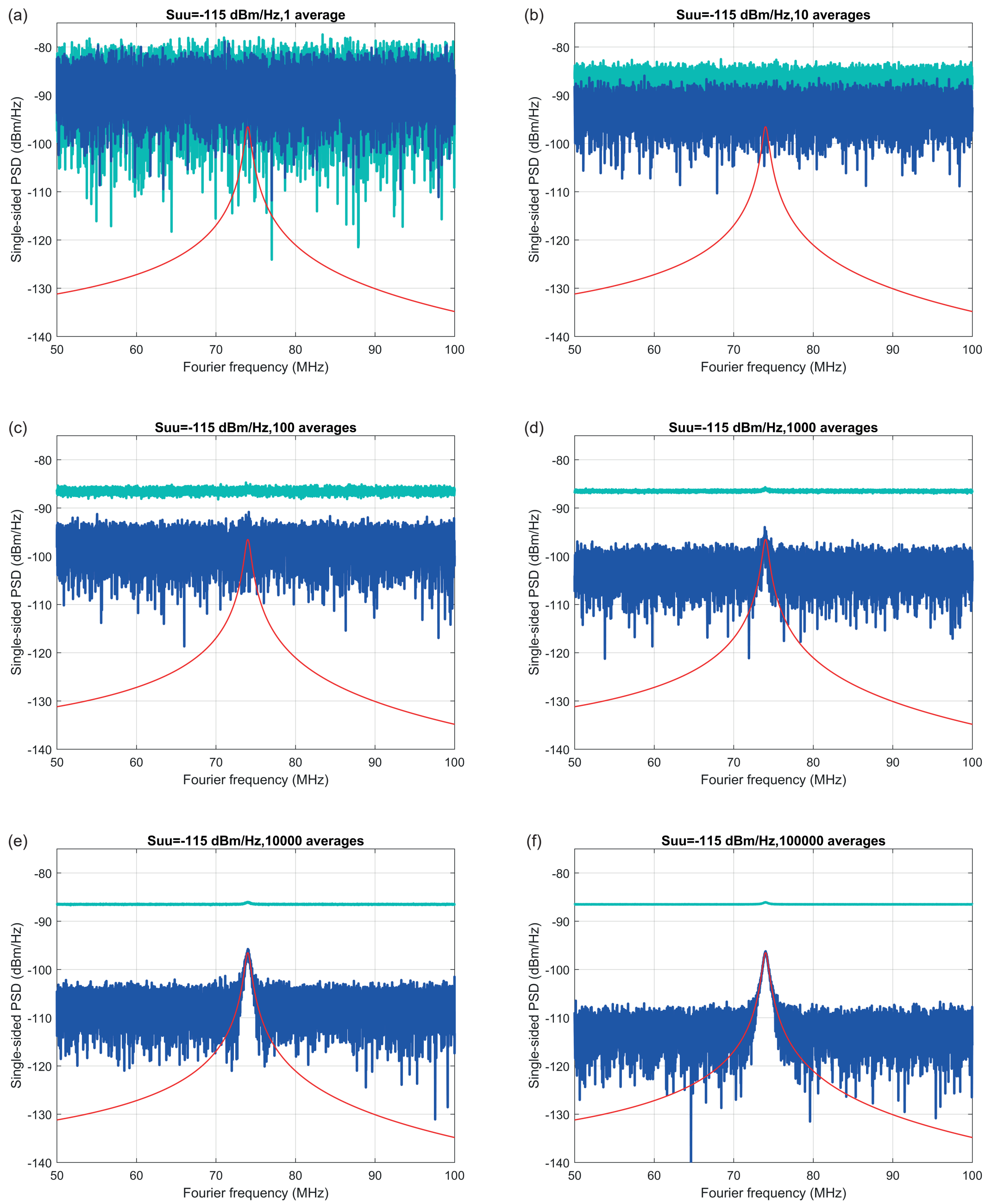

FIG. S6. Simulation of the Brownian motion of the resonator. $\langle S_{v_1v_1}\rangle_m$ (light blue) and $|\langle S_{v_2v_1}\rangle_m|$ (dark blue) are shown as a function of Fourier frequency for m ranging from 1 to 10^5.

V. IN-PHASE AND QUADRATURE COMPONENTS OF VIBRATIONS

The vibrational phase ϕ_{m} estimated from in-phase and quadrature components of the photodetector output signal exhibits a linear dependence on drive frequency f_{d} away from resonance. It is attributed to propagation delay through the cables. We correct $\phi_{\mathrm{m}}(f_{\mathrm{d}})$ by subtracting off this linear dependence. Figure S7a displays $\phi_{\mathrm{m}}(f_{\mathrm{d}})$ obtained with approach (i) based on analog demodulation with SDRlab using two mixers and two local oscillators in quadrature. Figure S7b displays $\phi_{\mathrm{m}}(f_{\mathrm{d}})$ obtained with approach (ii) based on digital demodulation with SDRlab using one mixer and one local oscillator and IQ demodulation in software. Figure S7c displays $\phi_{\mathrm{m}}(f_{\mathrm{d}})$ obtained with approach (iii) based on digital demodulation with oscilloscope and IQ demodulation in software. Top (bottom) row shows uncorrected (corrected) ϕ_{m}.

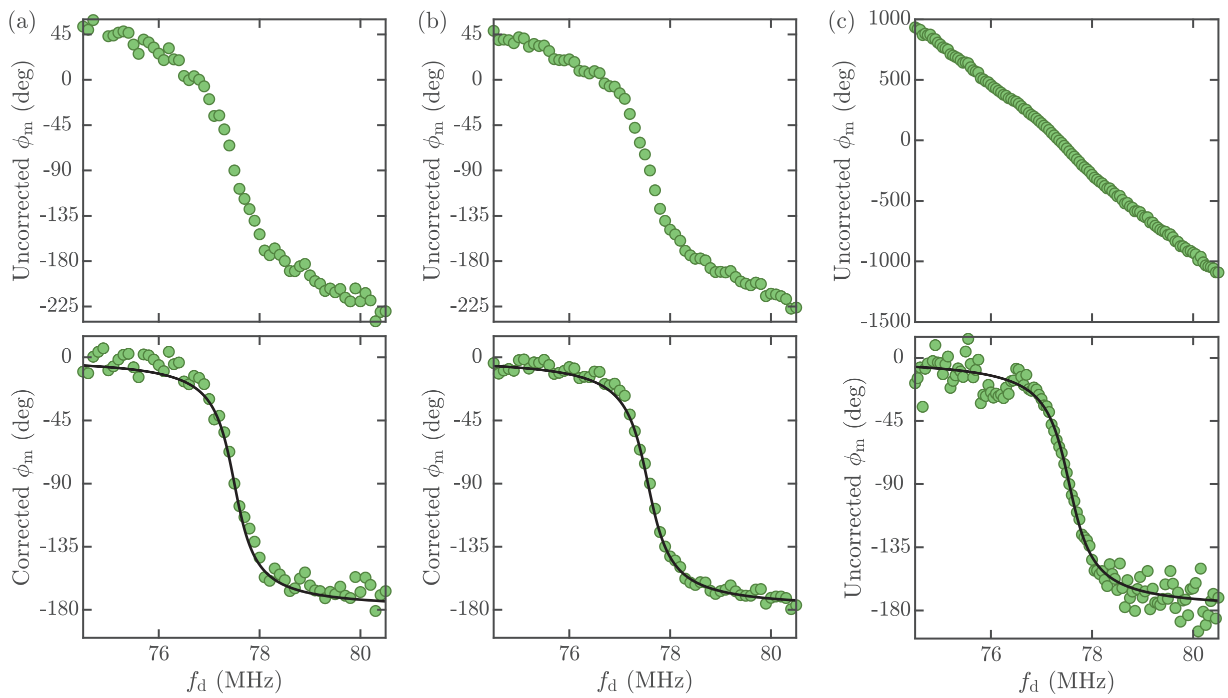

FIG. S7. Correcting the vibrational phase ϕ_{m}. (a) Approach (i). (b) Approach (ii). (c) Approach (iii). Black traces are fits to the response of a harmonic oscillator. $P_{\mathrm{d}} = -40$ dBm, $V_{\mathrm{g}}^{\mathrm{dc}} = -15$ V.

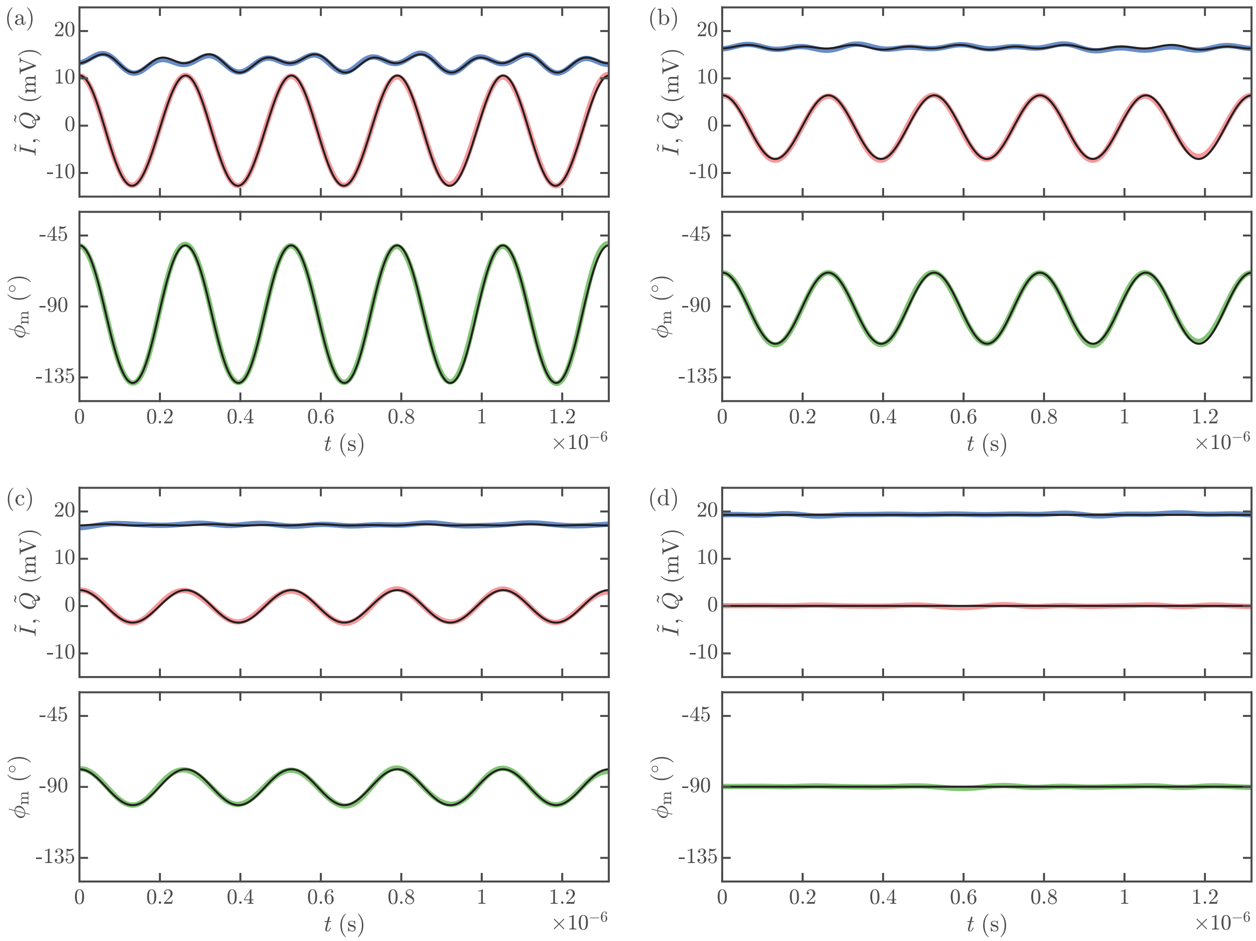

FIG. S8. $\tilde{I}$, $\tilde{Q}$ and ϕ_{m} as a function of time for $f_{\mathrm{mod}} = 3.8$ MHz and for $\kappa = 0.08$ (a), $\kappa = 0.04$ (b), $\kappa = 0.02$ (c), and $\kappa = 0$ (d).

VI. PHASE MODULATION INDUCED BY STRAIN MODULATION

Details of the dynamics of $\tilde{I}$ and $\tilde{Q}$ for various spring constant modulation strengths κ and modulation frequencies f_{mod} are shown in Figs. S8, S9, S10, and S11, where $P_{\mathrm{d}} = -40$ dBm and $V_{\mathrm{g}}^{\mathrm{dc}} = -14.7$ V. Black traces are obtained by solving a linear equation of motion for the resonator that includes a modulated spring constant of the form $k_{\mathrm{m}}[1 - \kappa \cos(2\pi f_{\mathrm{mod}} t)]$. Figure S8 shows $\tilde{I}$, $\tilde{Q}$ and ϕ_{m} as a function of time for $f_{\mathrm{mod}} = 3.8$ MHz and for $\kappa = 0.08$ (a), $\kappa = 0.04$ (b), $\kappa = 0.02$ (c), and $\kappa = 0$ (d). Similarly, Figure S9 is for $f_{\mathrm{mod}} = 7.6$ MHz, Fig. S10 is for $f_{\mathrm{mod}} = 9.5$ MHz, and Fig. S11 is for $f_{\mathrm{mod}} = 15.2$ MHz.

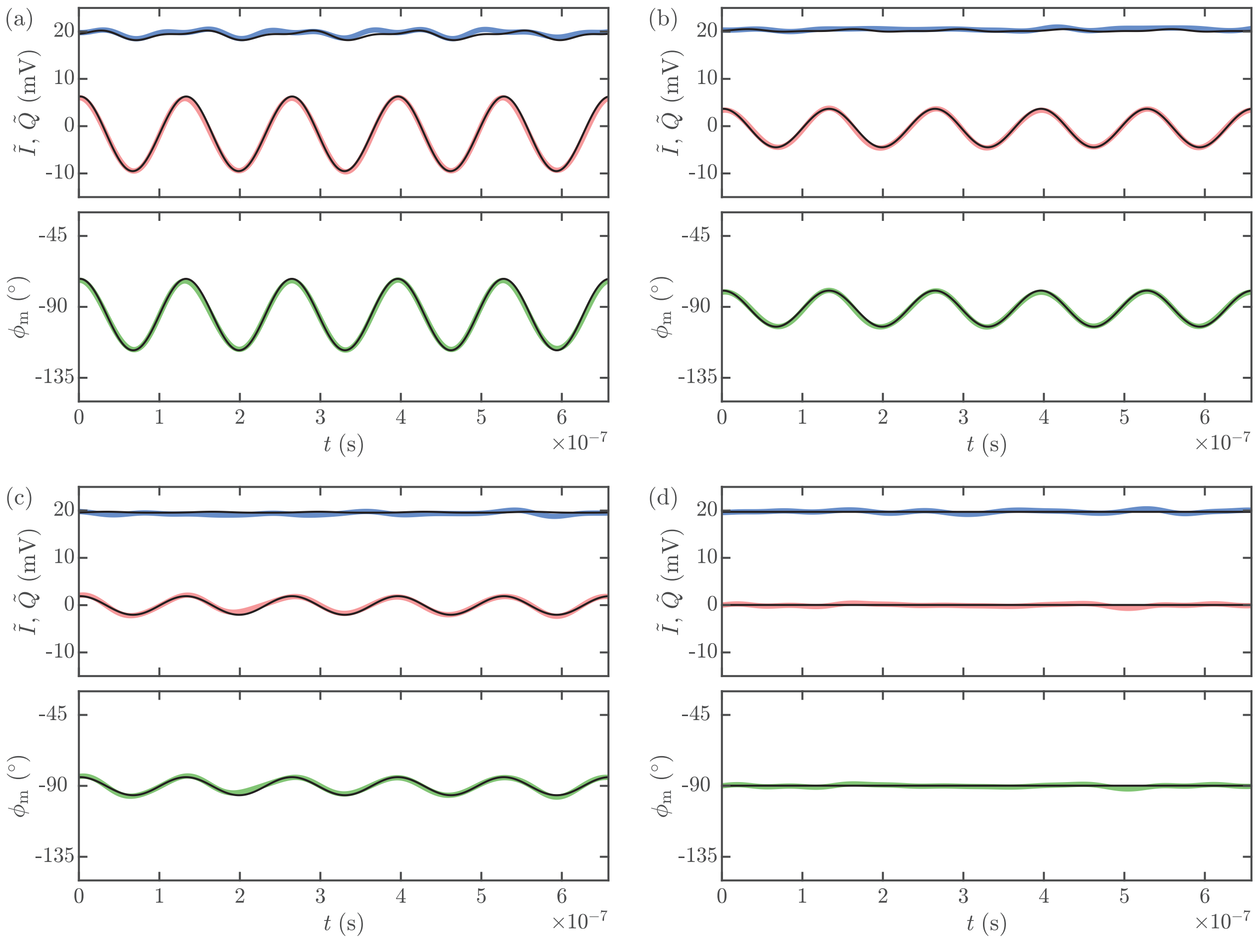

FIG. S9. $\tilde{I}$, $\tilde{Q}$ and $\phi_{\rm m}$ as a function of time for $f_{\rm mod} = 7.6$ MHz and for $\kappa = 0.08$ (a), $\kappa = 0.04$ (b), $\kappa = 0.02$ (c), and $\kappa = 0$ (d).

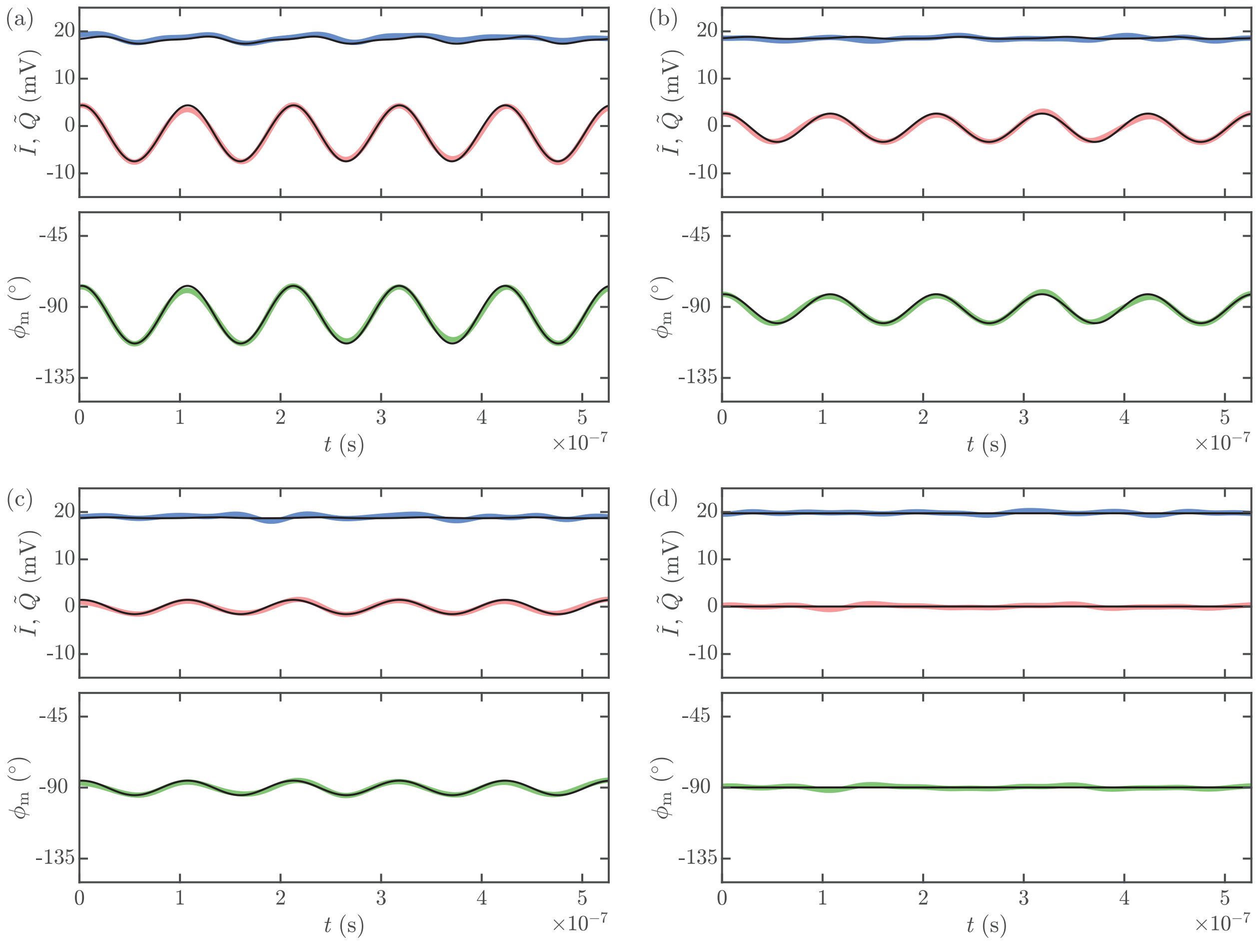

FIG. S10. $\tilde{I}$, $\tilde{Q}$ and $\phi_{\rm m}$ as a function of time for $f_{\rm mod} = 9.5$ MHz and for $\kappa = 0.08$ (a), $\kappa = 0.04$ (b), $\kappa = 0.02$ (c), and $\kappa = 0$ (d).

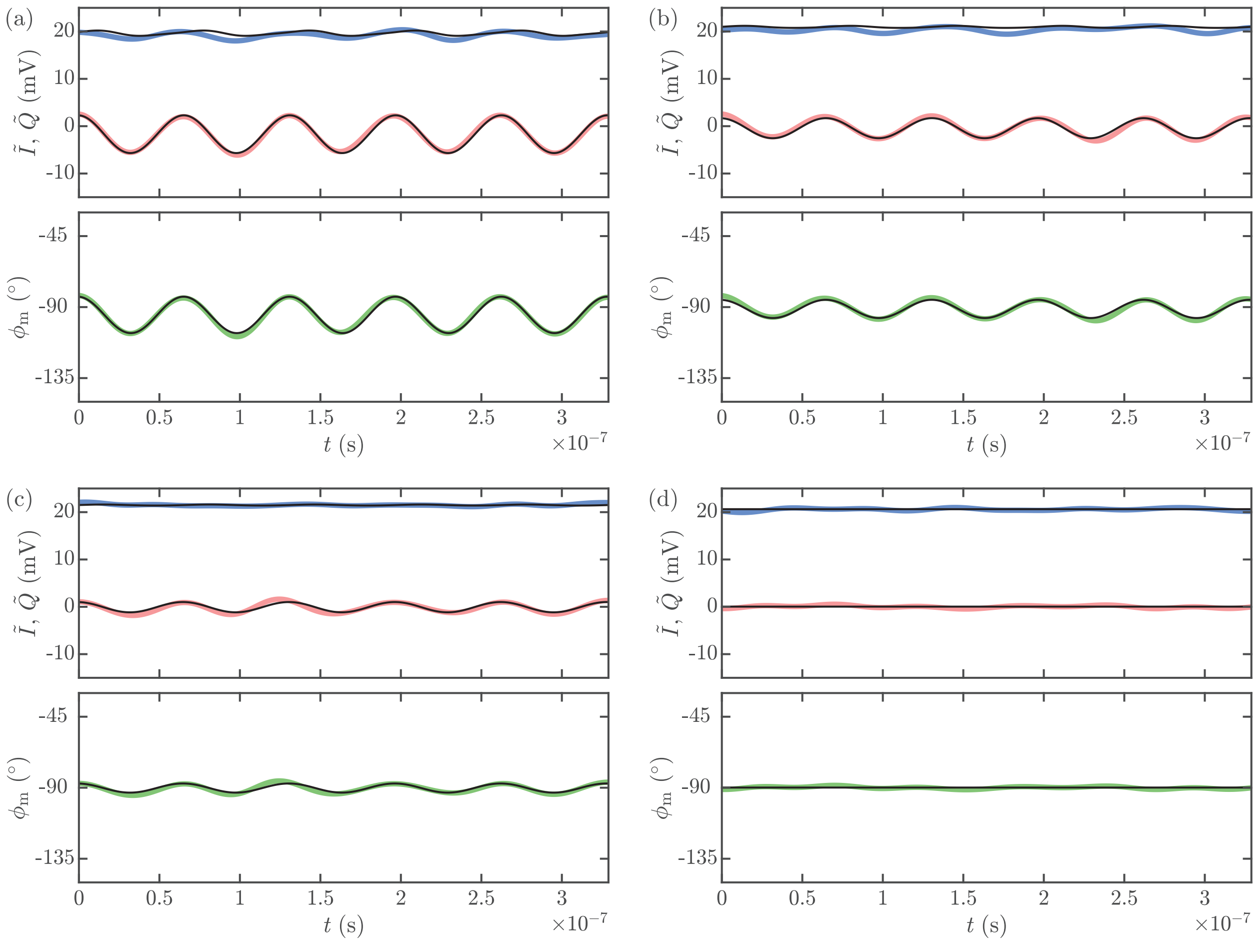

FIG. S11. $\tilde{I}$, $\tilde{Q}$ and ϕ_m as a function of time for $f_\mathrm{mod} = 15.2$ MHz and for $\kappa = 0.08$ (a), $\kappa = 0.04$ (b), $\kappa = 0.02$ (c), and $\kappa = 0$ (d).

Figure S12 displays simulations showing the effect of f_mod on the dynamics of in-phase I and quadrature Q components of vibrations. Parameters are $f_\mathrm{m} = 76$ MHz, $Q_\mathrm{m} = 110$, $m_\mathrm{eff} = 10^{-17}$ kg, $P_\mathrm{d} = -40$ dBm, and $V_\mathrm{g}^\mathrm{dc} = -14.7$ V. Geometrical parameters of the resonator in the main text are used. The spring constant modulation strength is $\kappa = 0.02$. Fig. S12a maps I and Q over a short time span for $f_\mathrm{mod} = 10^4$ Hz (black trace). The arc in red shows the extent of vibrational phase modulation amplitude $2\Delta\phi_\mathrm{m}$. The circle in grey maps in-phase and quadrature components of vibrations without modulation at $\kappa = 0$, $(f_\mathrm{m}^2 - f_\mathrm{d}^2)/D \times \sqrt{2}\delta F_\mathrm{d}/m_\mathrm{eff}$ and $(f_\mathrm{m} f_\mathrm{d}/Q_\mathrm{m})/D \times \sqrt{2}\delta F_\mathrm{d}/m_\mathrm{eff}$, with $D = (f_\mathrm{m}^2 - f_\mathrm{d}^2)^2 + (f_\mathrm{m} f_\mathrm{d}/Q_\mathrm{m})^2$, as f_d is swept through resonance. Figure S12b shows the power spectral density $S_{\phi\phi}$ of ϕ_m as a function of Fourier frequency f normalized to f_mod. At such low f_mod, ϕ_m swings to large values and the phase response is nonlinear. Figures S12c, d show the same analysis for $f_{\rm mod} = 10^5$ Hz. Figures S12e, f are for $f_{\rm mod} = 10^6$ Hz. Figures S12g, h are for $f_{\rm mod} = 2 \times 10^6$ Hz. Figures S12i, j are for $f_{\rm mod} = 4 \times 10^6$ Hz.

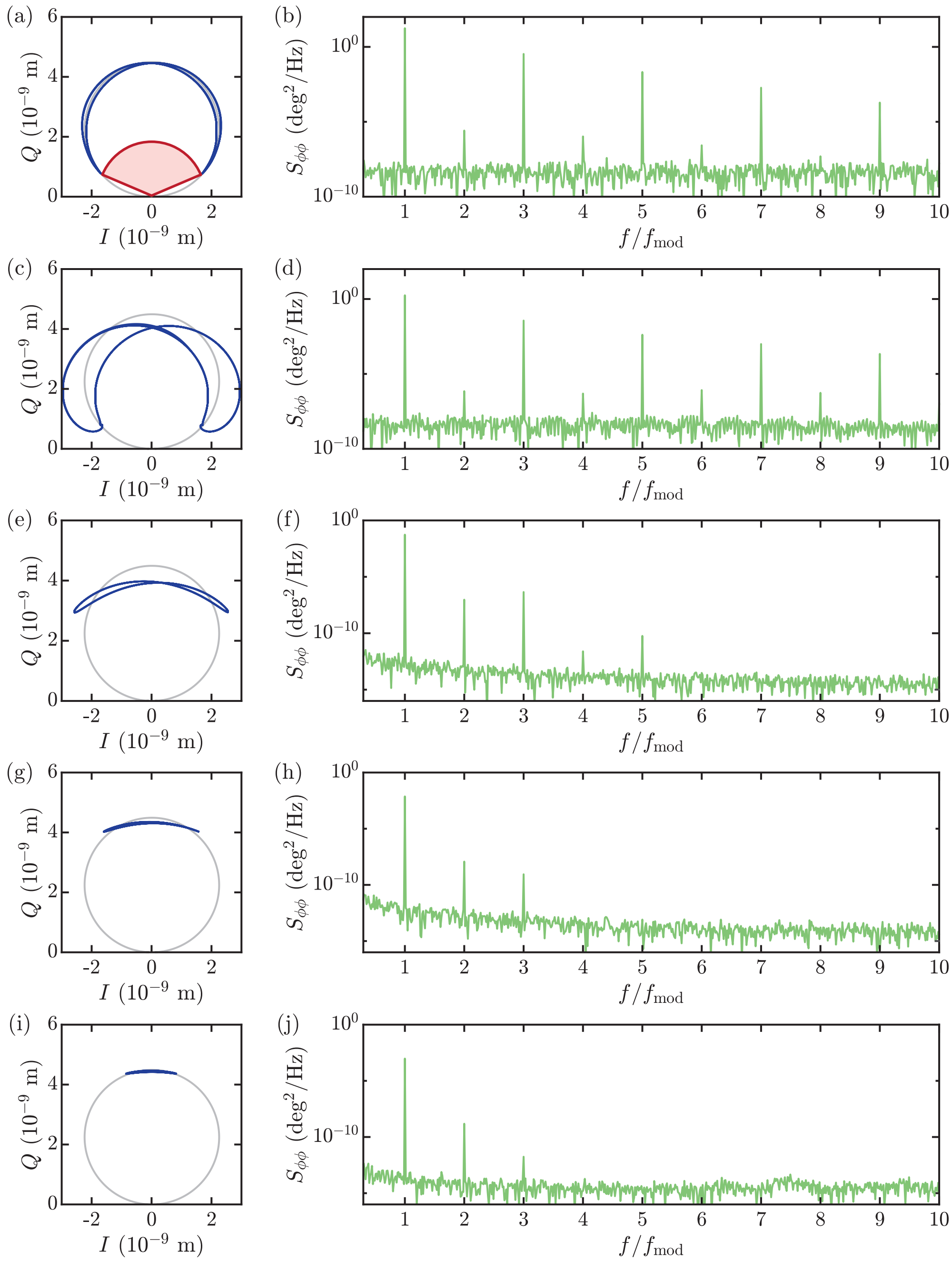

FIG. S12. Calculated in-phase I and quadrature Q components of vibrations and power spectral densities of vibrational phase $S_{\phi\phi}$ for modulation strength $\kappa = 0.02$. (a, b) $f_{\rm mod} = 10^4$ Hz. (c, d) $f_{\rm mod} = 10^5$ Hz. (e, f) $f_{\rm mod} = 10^6$ Hz. (g, h) $f_{\rm mod} = 2 \times 10^6$ Hz. (i, j) $f_{\rm mod} = 4 \times 10^6$ Hz.

VII. A NANOMECHANICAL TELEVISION BROADCAST

Two videos in mp4 format accompagny this Supplemental Material. Both are nanomechanical responses of our few-layer graphene resonator to QPSK modulated DVB-S waveforms produced with GNU Radio [5]. They are made by demodulating I, Q data at the output of our SDR dongle using leandvb, an open-source DVB-S demodulator software [6]. The demodulated signal is then converted into a video in mp4 format using FFmpeg, an open-source software for processing multimedia files [7]. The first video (9june4-10-61.mp4) shows our lab with some of the authors at work, with a musical background. The second video (9june5-44-63.mp4) contains human voice and shows the corresponding author's son. Figure S13a (b) shows a snapshot from the first (the second) video.

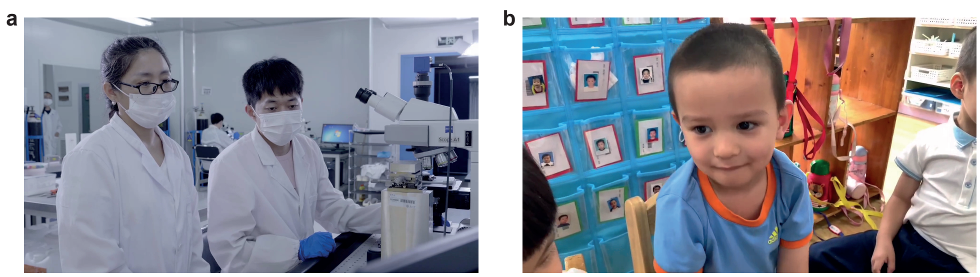

FIG. S13. A nanomechanical television broadcast. (a) Snapshot from 9june4-10-61.mp4. (b) Snapshot from 9june5-44-63.mp4.

[1] Roddaro, S., Pingue, P., Piazza, V., Pellegrini, V. & Beltram, F. The optical visibility of graphene: Interference colors of ultrathin graphite on SiO_2. *Nano Lett.* **7**, no. 9, 2707–2710 (2007).

[2] Wang, Z. & Feng, P.X.-L. Interferometric motion detection in atomic layer 2D nanostructures: visualizing signal transduction efficiency and optimization pathways. *Sci. Rep.* **6**, 28923 (2016).

[3] Storch, I. R., De Alba, R., Adiga, V. P., Abhilash, T. S., Barton, R. A., Craighead, H. G., Parpia, J. M. & McEuen, P. L. Young's modulus and thermal expansion of tensioned graphene membranes. *Phys. Rev. B* **98**, no. 8, Art. no. 085408 (2018).

[4] Nørrelykke, S. F. & Flyvbjerg, H. Harmonic oscillator in heat bath: Exact simulation of time-lapse-recorded data and exact analytical benchmark statistics. *Phys. Rev. E* **83**, 041103 (2011).

[5] GNU Radio. https://www.gnuradio.org (2023)

[6] leandvb. http://www.pabr.org/radio/leandvb/leandvb.en.html (2023)

[7] FFmpeg. https://ffmpeg.org (2023)